

# Smartphone-Based Luminescent Thermometry via Temperature-Sensitive Delayed Fluorescence from $\text{Gd}_2\text{O}_2\text{S}:\text{Eu}^{3+}$

Ngei Katumo, Guojun Gao, Felix Laufer, Bryce S. Richards, and Ian A. Howard\*

Thermal images generated from infrared radiation are useful for monitoring many processes; however, infrared cameras are orders of magnitude more expensive than their visible counterparts. Methods that allow visible cameras to capture thermal images are therefore of interest. In this contribution, thermal images of a surface coated with an inexpensive inorganic micropowder phosphor are generated from the analysis of a video taken with a smartphone camera. The phosphor is designed to have a temperature-dependent emission lifetime that is long enough to be determined from the analysis of a 30 frames-per-second video recording. This proof-of-principle work allows temperatures in the 270–320 K range to be accurately determined with a precision better than 2 K, even in the presence of bright background illuminance up to  $1500 \text{ lm m}^{-2}$ . In the broader context, this inspires further development of phosphors to bring time-resolved sensing techniques into lifetime long enough ranges to allow smartphone-based detection.

## 1. Introduction

Materials whose luminescence properties change as a function of temperature can be used as thermometers to precisely determine temperatures in hard-to-access locations, including biological, and analytical systems.<sup>[1]</sup> If these materials are distributed in a 3D volume or over a 2D surface, camera-based imaging techniques can rapidly create spatial maps of local temperature, a process known as optical thermography. The


development of nanoscale luminescent thermometers and their use in fluorescent microscopes is leading to great success in allowing temperature to be imaged in vivo at the microscale in biological systems. This has significant implications not only for fundamental understanding and diagnosis, but also for guiding therapeutic actions such as photothermal therapy.<sup>[1b,2]</sup> However, in these cases, the basis for the temperature sensing is typically on a temperature-induced change in emission intensity (or intensity ratio between two peaks). This means that background radiation in these wavelength regions must be carefully controlled; a task possible in a fluorescence microscopy setup, but not easily achievable in everyday situations. Instead, temperature-induced changes in emission lifetime can also be used to

establish temperature. Such temporal-based detection is less sensitive to environmental variables such as different absorption or scattering of the luminescent thermometer emission (or the excitation light).<sup>[2d,3]</sup> However, in existing material systems these advantages are outweighed by the cost of the high-speed imaging equipment needed to capture the approximately microsecond lifetimes of the materials. For certain applications—such as monitoring of surface temperatures in internal combustion or gas turbine engines used in aircraft propulsion—the high cost of cameras with frame rates exceeding 500 kHz can be justified, and 2D temperature images can be reconstructed from analysis of these very high frame rate videos.<sup>[4]</sup>

Herein, we present a phosphor that allows smartphone cameras to produce 2D temperature images. This smartphone thermal imaging (or thermography) is accomplished using delayed luminescence lifetimes longer than 100 ms that are accurately determinable from analysis of a smartphone video. This work supports the broader trend in the literature to bring techniques that have thus far been accessible only in controlled laboratory setting with dedicated (expensive) equipment into an accessible and inexpensive format to allow more general application. In terms of smartphone-based temperature sensing, recent work by Ramalho et al. demonstrated a smartphone-based ratio-metric approach to smartphone-based temperature determination that used luminescent quick response (QR) codes based on binuclear complexes of  $\text{Eu}^{3+}$  and  $\text{Tb}^{3+}$ .<sup>[5]</sup> By analyzing the shift in the histogram for the red and green channels after ultraviolet (UV) excitation, they were able to determine the temperature of

N. Katumo, Dr. G. Gao, F. Laufer, Prof. B. S. Richards, Dr. I. A. Howard  
Institute of Microstructure Technology  
Karlsruhe Institute of Technology  
Hermann-von-Helmholtz-Platz 1, Eggenstein-Leopoldshafen 76344,  
Germany  
E-mail: [ian.howard@kit.edu](mailto:ian.howard@kit.edu)

F. Laufer, Prof. B. S. Richards, Dr. I. A. Howard  
Light Technology Institute  
Karlsruhe Institute of Technology  
Engesserstrasse 13, Karlsruhe 76131, Germany

 The ORCID identification number(s) for the author(s) of this article can be found under <https://doi.org/10.1002/adom.202000507>.

© 2020 The Authors. Published by WILEY-VCH Verlag GmbH & Co. KGaA, Weinheim. This is an open access article under the terms of the Creative Commons Attribution-NonCommercial-NoDerivs License, which permits use and distribution in any medium, provided the original work is properly cited, the use is non-commercial and no modifications or adaptations are made.

DOI: [10.1002/adom.202000507](https://doi.org/10.1002/adom.202000507)

the label between 283–317 K with an impressive average sensitivity of 5%/K and a temperature resolution better than 0.2 K.<sup>[5a]</sup> Earlier work showed temperature sensing at the tip of a fiber probe was possible with a diffraction grating and smartphone (range of 263–453 K).<sup>[6]</sup> More broadly, there is a broad and successful ongoing literature demonstrating the effectiveness of quantitative analysis of photoluminescence (PL) intensity or color with a smartphone for chemical assays,<sup>[7]</sup> and anti-counterfeiting purposes.<sup>[8]</sup> For example, a lateral flow assay using SrAl<sub>2</sub>O<sub>4</sub>:Eu<sup>2+</sup>,Dy<sup>3+</sup> nanophosphors with persistent luminescence allowed the intensity of light emitted in the test and control strips to be quantitatively determined after the smartphone flash excitation was turned off.<sup>[7b]</sup>

Beyond these intensity-based methods, two recent reports deal with the determination of PL lifetime using a smartphone.<sup>[9]</sup> The first develops a method to measure lifetimes far faster than the frame rate of the camera by translating the time dimension into a spatial dimension.<sup>[9b]</sup> By placing the sample on a rapidly rotating disc, the emission lifetime is converted into a “streaked” spatial arc, allowing sub-millisecond lifetimes to be determined (but without spatial resolution).<sup>[9b]</sup> More interestingly for our purposes, it was recently shown that the approximately 300 ms lifetime of room temperature phosphorescence from an organic material can be easily determined by the analysis of a smartphone video, as can its changing lifetime with oxygen concentration in order to enable oxygen sensing.<sup>[9a]</sup> Herein we show that robust inorganic phosphors can also be designed to bring the benefits of life-time based sensing to a smartphone platform.

We demonstrate that the delayed luminescence from charge-transfer states in europium doped gadolinium oxysulfide (Gd<sub>2</sub>O<sub>2</sub>S:Eu<sup>3+</sup>) provides a temperature-dependent lifetime on the order of hundreds of milliseconds. This allows thermal images to be created via the analysis of video captured using a standard smartphone camera at a rate of 30 frames-per-second (fps). The optical excitation is provided using a sub-Hz modulated UV light-emitting diodes (UV LED, 375 nm) making the entire system very economical. Further development should allow delayed-luminescence thermometry materials to be excited directly with the smartphone flash (i.e., have absorption bands up to 450 nm), opening possibilities for thermal imaging using exclusively a smartphone for both excitation and detection. The present work, and the recent results demonstrating smartphone-based lifetime sensing of oxygen using long-lived room-temperature phosphorescence,<sup>[9a]</sup> show it is possible to translate various lifetime sensors to a regime that enables smartphone-based PL lifetime detection.

To date, phosphors for lifetime-based thermometry have had lifetimes typically much less than 10 ms, making it impossible to measure the lifetime with a 30-fps camera. A broad range of luminescent materials—such as lanthanides,<sup>[2d]</sup> organic-inorganic compounds,<sup>[10]</sup> carbon dots,<sup>[11]</sup> organic molecules,<sup>[12]</sup> nitrogen-vacancy centers in diamond,<sup>[13]</sup> and dual emitter systems<sup>[14]</sup>—have already been explored for thermometry based on either PL intensity ratio or lifetime parameters. Indeed, commercial products have been available since the 1980s that use the luminescence from phosphor-coated fiber tips to determine temperature.<sup>[15]</sup> Whereas first generations of these technologies used intensity ratios from Gd<sub>2</sub>O<sub>2</sub>S:Eu<sup>3+</sup>,<sup>[15a]</sup> subsequent generations switched to the more robust lifetime measurement method, using the millisecond emission lifetimes of phosphors such as

manganese-doped magnesium fluorogermanate.<sup>[15b]</sup> Although lifetimes <10 ms can be determined inexpensively by single-pixel detectors, their use in thermal imaging requires expensive equipment such as an ultra-high speed camera.

Gd<sub>2</sub>O<sub>2</sub>S is an extensively studied phosphor host well-known to provide excellent PL quantum yields via X-ray, cathode-ray, or UV excitation.<sup>[16]</sup> For applications such as X-ray imaging, afterglow (delayed luminescence) must be minimized in the phosphor to prevent ghosting between images on the CCD.<sup>[17]</sup> In this work, we demonstrate how these previous perceived disadvantages of the phosphor (delayed luminescence and temperature sensitivity) can be capitalized upon to realize smartphone-based luminescent lifetime thermometry. As a first step, we synthesized a sequence of Gd<sub>2</sub>O<sub>2</sub>S: *x* % Eu<sup>3+</sup> phosphors with *x* varying from 1 to 13 mol%. X-ray diffraction patterns for the materials and a scanning electron microscope image are shown in Figure S1, Supporting Information. Basic optical characterization of the material series is summarized in Figure S2, Supporting Information. We observed that, at room temperature, the PL quantum yield was highest and the delayed luminescence lifetime was longest for the 6% sample, and therefore selected this material for the following investigations.

## 2. Results and Discussion

**Figure 1** demonstrates how a smartphone video can be used to accurately determine the lifetime of the phosphor’s delayed emission lifetime. In Figure 1a, the setup for acquiring the smartphone video is illustrated. A sample of the Gd<sub>2</sub>O<sub>2</sub>S:6% Eu<sup>3+</sup> material is placed in a small crucible on a temperature-controlled stage (MHCS622, Microptik) and, in this case, held at 273 K. The temperature of the phosphor in the crucible can be varied by heating/cooling the stage. A current controller (ITC4001, Thorlabs) is used to create square wave “flashes” from a 375 nm UV LED (XSL 375, Roithner LaserTechnik). The UV LED was on for 1000 ms, then off for 9000 ms. A smartphone (Galaxy A5 (2017), Samsung Electronics) was used to record video using a third-party app (Camera HD, Mark Harman). The video was recorded at 30 frames per second and then imported into MATLAB for subsequent analysis. Figure 1a shows a sequence of individual frames extracted from the video, with frame 0 being the last frame in which the UV LED was still on. As can be seen, emission from the phosphor is clearly visible in the individual frames, even long after the UV LED has been switched off. The excitation power density was 25 mW cm<sup>-2</sup>, and did not induce sample heating (see Figure S3, Supporting Information).

The lifetime of the delayed emission can be determined from the smartphone video in the following fashion. For each frame, the value of the red-channel (a number between 0 and 255) is summed over a region of interest (in this case the circular area of the crucible). This “intensity” value for the luminescence is then placed at the time of the relevant frame, and data such as those presented in Figure 1b are obtained. Several times of interest are also noted. The first frame after the UV excitation is turned off is found by searching for the maximum difference between subsequent two frames. This frame is labeled as *t*<sub>0</sub>. Then, the time window in which the data will be fit in order to estimate the lifetime (*t*<sub>1</sub> – *t*<sub>2</sub>) is determined. The first value, *t*<sub>1</sub>,

is simply a constant offset from  $t_0$  to allow for settling of the instrument response of the system from the rapid decrease in the prompt luminescence. This is taken to be 221 ms for all measurements, meaning that, in all cases,  $t_1$  is simply 221 ms after  $t_0$ . Determining the second value,  $t_2$ , is slightly more involved. It is the time at which 90% of the total delayed emission has been collected, and is found automatically as described in the Supporting Information (Figure S4, Supporting Information). As seen later,  $t_2$  varies with the delayed decay lifetime and therefore temperature. The delayed decay lifetime,  $\tau$ , is then estimated by an exponential fit of the form  $y = A \exp\left(-\frac{t}{\tau}\right)$  to the data between  $t_1$  and  $t_2$ . At 293 K (room temperature), the lifetime of the delayed emission extracted from the video-recorded PL emission was  $475 \pm 13$  ms. The lifetime extracted from the smartphone video agrees with the lifetime measured by single-photon counting and multichannel scaling ( $484 \pm 4$  ms), albeit the lifetime determined from the smartphone exhibits an

uncertainty roughly a factor-of-three greater than that determined via single-photon counting measurements. Thus, we find that the delayed lifetime of these long-lived phosphors can be accurately estimated by the analysis of a smartphone video, and the precision of this method give a relative uncertainty of around 3% in the lifetime (at room temperature).

Figure 2a illustrates how the delayed PL lifetime (determined by analysis of smartphone videos) is strongly affected by temperature in the range from 273 to 333 K. Whereas significant delayed PL is readily apparent by eye for >50 frames at the lower temperatures, the signal disappears much more quickly for higher temperatures. A decrease in PL quantum yield and lifetime as temperature increases is typical for phosphors due to increased rates of non-radiative recombination at higher temperatures. However, this simple explanation cannot describe the mechanism responsible for the temperature dependence of the delayed emission in this phosphor. Instead, the delayed luminescence in  $\text{Gd}_2\text{O}_2\text{S}:\text{Eu}^{3+}$  relies on the thermal promotion of excitations held in a long-lived charge-transfer band to the  $^5\text{D}_0$  level of the  $\text{Eu}^{3+}$  ion.<sup>[18]</sup> As this radiative pathway for the delayed is temperature activated (along with the non-radiative pathways), the lifetime of the delayed emission decreases with increasing temperature but the PL quantum yield is reduced less than it would be if only the non-radiative channel were temperature activated. This is beneficial in allowing the delayed luminescence to remain bright enough for its lifetime to be measured as the temperature is increased. As a side note, the PL intensity of these materials does not monotonically decrease with increasing temperature (as would a material whose temperature dependence is caused by the activation of a non-radiative rate), see Figure S5, Supporting Information. A description of the temperature-dependent charge-transfer band model that describes the photophysics of these phosphors is provided in Figure S6, Supporting Information.

Returning to the analysis of the data presented in Figure 2, the emission intensity (integrated over the crucible) as a function of time can be obtained by performing the analysis described above on the videos taken at the various temperatures. This yields data such as those plotted in Figure 2b from which the lifetime of the delayed luminescence as a function of temperature can be established. We took similar videos in five independent temperature sweeps, the other four datasets are shown in Figure S7, Supporting Information. The lifetime of the delayed luminescence as a function of temperature is presented in Figure 2c, with the error bars representing the standard deviation of the lifetimes extracted from five different trial videos taken at each temperature. The lifetimes in the 273–333 K temperature range can be well-fit with an equation of the form  $\tau(T) = A \exp\left(\frac{E_a}{k_B T}\right)$ , where  $k_B$  is the Boltzmann constant and  $E_a$  represents the apparent activation energy for the radiative and non-radiative rates. The value of  $E_a$  is determined to be  $0.29 \pm 0.01$  eV, while the prefactor  $A$  is found to be  $(4 \pm 1) \times 10^{-3}$ .

Using these calibration data and taking a measured lifetime, the temperature of the phosphor can be established simply by inverting the previous equation to  $T = \frac{E_a}{k_B(\ln(\tau) - \ln(A))}$ . Figure 2d displays the dependence of relative sensitivity ( $S_r$ ) as a function of temperature from 273 to 333 K. The relative

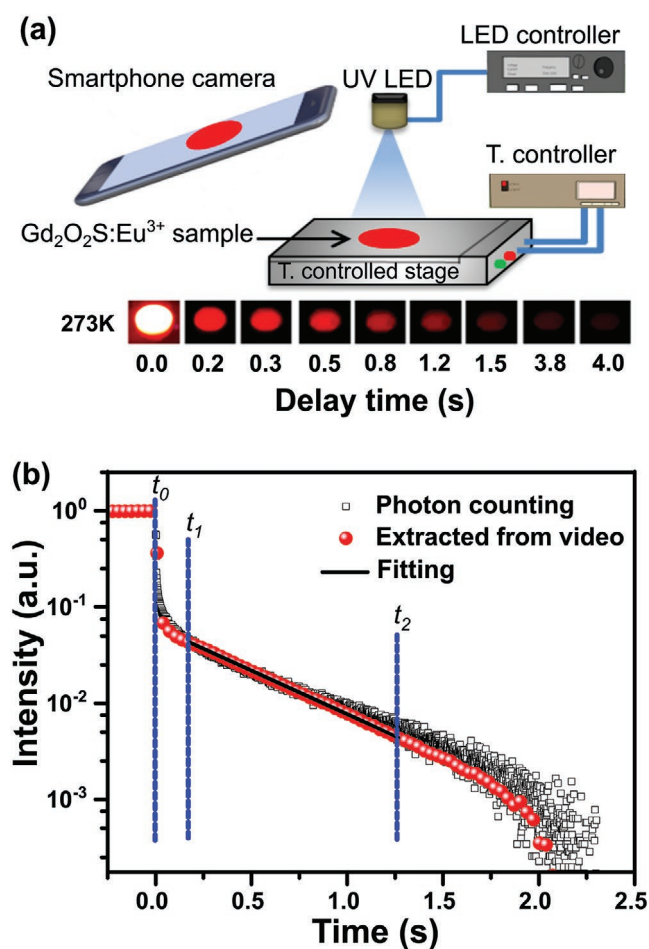


**Figure 1.** a) The experimental apparatus for recording videos of the delayed luminescence with a smartphone camera from the phosphor (at a given temperature) after modulated UV excitation. Single frames extracted from the video of the luminescence of  $\text{Gd}_2\text{O}_2\text{S}:\text{6\% Eu}^{3+}$  at 273 K, the UV illumination was turned off at time 0. b) The delayed luminescence lifetime of  $\text{Gd}_2\text{O}_2\text{S}:\text{6\% Eu}^{3+}$  at 293 K extracted from a smartphone video compared to reference data taken by conventional single-photon counting with a multi-channel scaler. The notations  $t_0$ ,  $t_1$ , and  $t_2$  are described in the text.

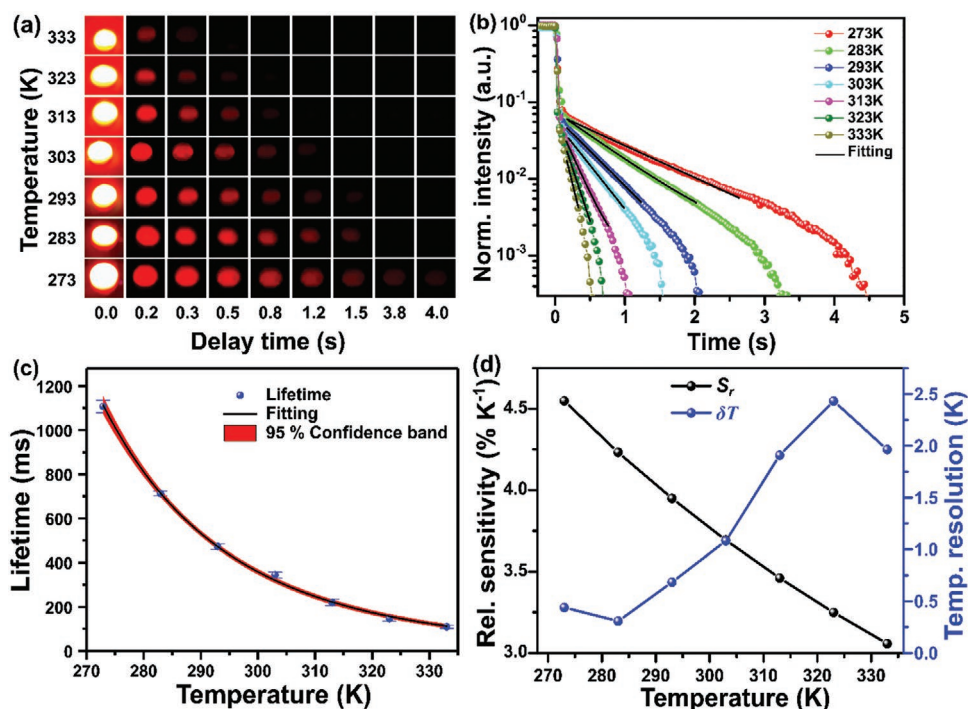


**Figure 2.** a) Individual frames extracted from videos of  $\text{Gd}_2\text{O}_2\text{S}:6\% \text{Eu}^{3+}$  as a function of temperature. b) Emission intensity (normalized) as a function of time extracted from videos of emission of  $\text{Gd}_2\text{O}_2\text{S}:6\% \text{Eu}^{3+}$  after pulsed UV LED excitation (375 nm) for various temperatures. c) Variation of the delayed luminescence lifetime as a function of temperature in the 273–333 K range. d) Relative sensitivity and temperature resolution.

sensitivity indicates by what percent the lifetime changes per degree change in temperature. This can be determined using  $S_r = \frac{E_a}{k_B T^2}$ ,<sup>[5a]</sup> and the values decrease from 4.5%  $\text{K}^{-1}$  at 273 K to 3.1%  $\text{K}^{-1}$  at 333 K. The temperature resolution ( $\delta T$ ), computed from  $= \frac{1}{S_r} \times \frac{\delta \tau}{\tau}$ , where  $\frac{\delta \tau}{\tau}$  is the relative standard error in the lifetime (which we found to be 2.6, 1.4, 2.7, 4.0, 6.7, 7.9, and 6.0% for 273, 283, 293, 303, 313, 323, and 333 K, respectively, based on the standard deviation of five repeated measurements at each temperature). The temperature resolution is better than 1 K for temperatures below 300 K, but then decreases to 2.5 K for temperatures around 333 K. The temperature resolution is best for lifetimes greater than 300 ms, and starts worsening as the lifetime drops below this. We find a practical limit of 100 ms for the minimum lifetime that we can determine based on smartphone video analysis of our phosphor. This corresponds to a maximum temperature around 338 K for our phosphor. The temperature range possible to measure could be expanded by increasing the frame-rate of the camera or developing further phosphors with temperature dependent lifetimes exceeding 100 ms in different temperature regimes.

We also note that an advantage of the lifetime-based approach is its relative insensitivity to background light. Whereas a ratio-metric measurement is disrupted when a background illumination alters the ratio between the two wavelength regions of interest, the measurement of the decay time of a material is not affected by background illumination. Given sufficient dynamic range of the detector, the background signal can simply be subtracted and it is only the background noise that degrades the lifetime determination. The measurements presented

in the main text are done in the dark, but in Figures S8–S12, Supporting Information we show that the lifetime measurements done at room temperature for room lighting conditions varying from 0 to 1500  $\text{lm m}^{-2}$  do not affect the lifetime determination. Here we used an inexpensive 650 nm short-pass filter (FESH0650, Thorlabs) and a 600 nm long-pass filter (FELH0600, Thorlabs) in front of the smartphone camera to reduce the effect of the background. With these filters in place, by 1500  $\text{lm m}^{-2}$  the background level is almost half of the intensity of the luminescence when the UV excitation is on. However, on our normalized scale the background noise remains less than  $3.5 \times 10^{-4}$  whereas our signal height is greater than  $1 \times 10^{-3}$ . Thus, the lifetime can be determined accurately irrespective of the background illumination at least up to those found in typical indoor lighting situations.

In order to test the accuracy of this approach of establishing the temperature at various locations along an object from a single video, we set up an inhomogeneous temperature gradient in a metal bar using two heating/cooling stages. One end of the bar was held at 270 K and the other was held at 320 K. In this way, a steady-state temperature profile with a gradual spatial variation was created along the bar. The bar had five patches along the plate where a thin layer of the phosphor powder material was pressed onto the bar. Adjacent to the middle of each patch, a thermocouple probe was attached to the bar in order to provide an independent measurement of the temperature at each location. A strip of six UV LEDs (375 nm) were employed to uniformly illuminate the surface of the plate. This apparatus is schematically illustrated in Figure 3a.

Figure 3b shows individual frames extracted from a smartphone video of the entire plate after the UV LEDs light strip was

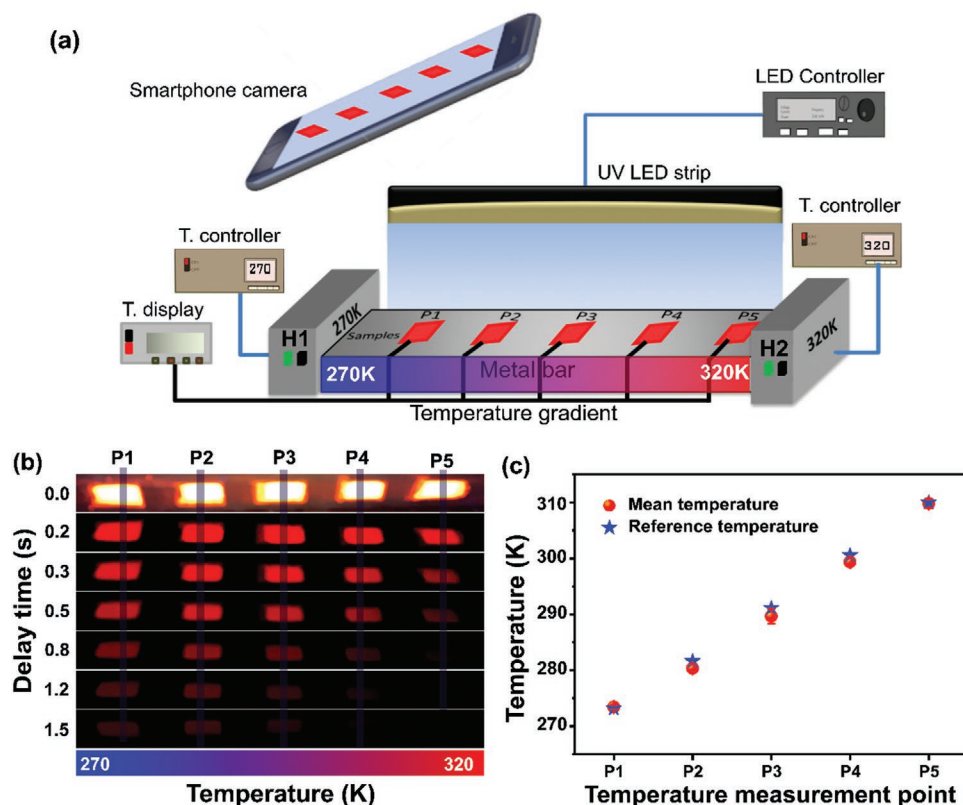


**Figure 3.** a) Experimental apparatus for establishing a temperature gradient from 270 to 320 K along a metal bar. The bar has a patch of phosphor material and a thermocouple at five locations along its length. The bar is uniformly illuminated using several UV LEDs and the emission detected using a smartphone camera. b) Individual frames from an exemplary smartphone video showing that delayed emission is visible from the cold side of the bar much longer than it is from the hot side of the bar. c) The temperatures estimated from the smartphone-established lifetime are shown for each of the five points on the metal bar (note five separate videos were taken, red circles represent mean temperature extracted from lifetimes of the individual videos). These are compared with the reference value read from the thermocouple at that location (blue star).

turned off (with again frame 0 being the last frame in which the UV LEDs were still on). In the early frames, the emission from all patches on the bar is similar. However, in the later frames, the emission from the hotter side of the bar rapidly fades away leaving only the longer delayed emission from the cooler side of the bar. By integrating the emission intensity over each patch of phosphor, the delayed emission lifetime at these five points can be established from a single video. We established the lifetime in this fashion for each of the five points and converted it into a temperature using the above relationship. We did this for five independent videos. The resulting estimated temperatures are shown in Figure 3c and compared to the reference temperature measured by the thermocouple. In each case, the reference value lay within the error bars of the measured temperature.

Analyzing the spread of the lifetimes measured in subsequent videos, the average resolution in the temperatures determined by the phosphor lifetime was 0.9 K (full data shown in Table S1, Supporting Information). In contrast, the average deviation between the temperature measured with phosphor lifetime and the reference thermocouple was 0.6 K. Therefore, the accuracy of the technique is good, with the real temperature falling within the resolution range of the lifetime-established temperature in each case. Also, the precision of around 1 K agrees well with the temperature resolution predicted in Figure 2d.

The results shown herein are for pure phosphor powders applied to a surface. However, we can also measure lifetimes with the smartphone when the phosphor is held in a binder matrix at concentrations higher than 4% by weight in roughly 0.1 mm thick films (see Figure S14).

These results demonstrate the potential for lifetime-based sensing based on smartphone cameras, and also establish directions for further improvement. In order to achieve sensing over a wider temperature range, phosphors with a longer maximum lifetime would be desirable. With the range of persistent emission phosphors already developed (both inorganic and organic),<sup>[19]</sup> such elongation of the lifetime is certainly possible. However, there is a trade-off in that moving to longer lifetimes also requires longer excitation pulses and videos to be taken (thereby slowing down the thermal image acquisition). The relative sensitivity that we demonstrate compares favorably with many existing luminescent thermometry approaches,<sup>[2d]</sup> however more precise temperature determination over a smaller temperature window should be possible with exploration of wide variety of potential phosphors, including novel organic materials.<sup>[20]</sup> The temperature resolution that we achieve is comparable to the 1–2 K temperature resolution typical for thermal imaging infrared cameras used for predictive maintenance of electrical equipment.<sup>[21]</sup> Also, in terms of application

in predictive maintenance of electrical equipment, the working range of our system to 330 K would be sufficient for a wide variety of cases.<sup>[22]</sup> Exploration and development of other phosphors have significant scope to tailor the range and sensitivity of smartphone-based thermal imaging, but we demonstrate that this first prototype already possesses sufficient figures-of-merit to compete with commercial products in the major application field of predictive maintenance.

### 3. Conclusion

In summary, we demonstrated smartphone-based luminescence imaging based on the delayed emission from  $\text{Gd}_2\text{O}_2\text{S}:\text{Eu}^{3+}$  phosphor. Temperatures in the range of 270–320 K can be determined with a temperature resolution better than 2 K, even at bright ambient light levels of  $1500 \text{ lm m}^{-2}$ . These promising results suggest that our approach could compete with commercial solutions used in thermal imaging for predictive maintenance. Taken in conjunction with recent work demonstrating the efficacy of a similar approach to visualize oxygen concentration due to its quenching of delayed luminescence,<sup>[9a]</sup> our results suggest that the development of special phosphors to enable smartphone-based lifetime detection that complement the existing strategies based on analysis of absolute PL intensities or colors.<sup>[7]</sup> Lifetime-based strategies can be made relatively insensitive to (changing) background illuminance, and also could be applied in parallel to a ratiometric approach in order to develop orthogonal multi-dimensional sensors.

### 4. Experimental Section

**Synthesis of  $\text{Gd}_2\text{O}_2\text{S}:\text{Eu}^{3+}$ :** The  $\text{Gd}_2\text{O}_2\text{S}:\text{xEu}^{3+}$  samples,  $(\text{Gd}_{1-x}\text{Eu}_x)_2\text{O}_2\text{S}$  for  $(0\% \leq x \leq 13\%)$  molar ratio, were synthesized by flux-assisted solid-state reaction in a furnace system according to literature procedures.<sup>[23]</sup> The starting materials were  $\text{Gd}_2\text{O}_3$ , (ChemPur, 99.9%)  $\text{Eu}_2\text{O}_3$  (ChemPur, 99.9%) and sulfur (S), (ChemPur, 99+ %), with  $\text{Na}_2\text{CO}_3$  (ChemPur, 99+ %) and  $\text{K}_3\text{PO}_4$  (ChemPur, 99+ %), used as flux.

**Photoluminescence Quantum Yield:** The PL emission spectra were recorded using a spectrometer (AvaSpec-HS2048XL, Avantes) system attached to an integrating sphere (15-cm diameter, Labsphere) and a UV LED ( $\lambda = 375 \text{ nm}$ , 1 mW) excitation source. The absolute PL quantum yield was measured via the de Mello method.<sup>[24]</sup> In brief, the UV LED was directed into the integrating sphere connected to an optical fiber of 1-mm diameter (FP100URT, Thorlabs) for collecting the signal. The integrating sphere had a baffle immediately before the fiber for preventing direct illumination of the fiber from the UV LED and sample emissions. Measurements of the empty sphere, direct and indirect excitation spectra, direct and indirect emission spectra and black background were recorded, from which the PL quantum yield was calculated.

**Temperature Dependent PL:** The temperature-dependent PL spectra were obtained using a temperature-controlled thermal stage (MHCS622-V/G, Microptik) integrated with a high resolution (0.1 K) temperature controller (MTDC600, Microptik) and a liquid nitrogen cooling system (LN2-SYS, Microptik). The phosphor samples were placed in small alumina crucibles inside the sample chamber of the thermal stage (see Figure 1a). The emission was filtered by a long-pass filter (450 nm) and then collected with an optical fiber of 0.6-mm diameter (P/N78277, Newport) coupled with spectrometer (AvaSpec-ULS2048, Avantes).

**PL Lifetime Thermometry Experiments:** The temperature control was provided with the thermal stage as above but videos of the emission

between 273 K and 333 K in 10 K steps were recorded using a 16-megapixel smartphone camera (Galaxy A5 (2017), Samsung electronics) under excitation with a UV LED (375 nm) at a frequency of 0.1 Hz with a 10% duty cycle. The smartphone camera settings are described in the SOI. A wait time of 5 min at each set point allowed the sample temperature to stabilize before a video was taken. The video was then processed in Matlab to determine the decay lifetime in a pixel region as described in the Supporting Information. For surface temperature application tests, the  $\text{Gd}_2\text{O}_2\text{S}:\text{Eu}^{3+}$  samples were press filled into a specially made uniform aluminum bar with five pocket patches. Reference temperature thermocouples (K-type, Fuehler System) were installed in specific locations (P1–P5) as shown in Figure 3a to cross-reference the obtained temperature after video analysis.

### Supporting Information

Supporting Information is available from the Wiley Online Library or from the author.

### Acknowledgements

The authors gratefully acknowledge financial support by the Helmholtz Association—The Helmholtz Energy Materials Foundry (HEMF) and the Recruitment Initiative of BSR. N.K. thanks the German Academic Exchange Service DAAD for financial support and the Karlsruhe School of Optics and Photonics (KSOP) for training. Open access funding enabled and organized by Projekt DEAL.

### Conflict of Interest

The authors declare no conflict of interest.

### Keywords

charge-transfer band, delayed luminescence, fluorescence, luminescent thermometry, temperature sensing

Received: March 24, 2020

Revised: June 28, 2020

Published online:

- [1] a) R. G. Geitenbeek, J. C. Vollenbroek, H. M. H. Weijgertze, C. B. M. Tregouet, A. E. Nieuwelink, C. L. Kennedy, B. M. Weckhuysen, D. Lohse, A. van Blaaderen, A. van den Berg, M. Odijk, A. Meijerink, *Lab Chip* **2019**, *19*, 1236; b) B. del Rosal, E. Ximendes, U. Rocha, D. Jaque, *Adv. Opt. Mater.* **2017**, *5*, 1600508.
- [2] a) E. C. Ximendes, U. Rocha, T. O. Sales, N. Fernández, F. Sanz-Rodríguez, I. R. Martín, C. Jacinto, D. Jaque, *Adv. Funct. Mater.* **2017**, *27*, 1702249; b) H. D. A. Santos, E. C. Ximendes, M. d. C. Iglesias-de la Cruz, I. Chaves-Coira, B. del Rosal, C. Jacinto, L. Monge, I. Rubia-Rodríguez, D. Ortega, S. Mateos, J. García Solé, D. Jaque, N. Fernández, *Adv. Funct. Mater.* **2018**, *28*, 1803924; c) X. Zhu, W. Feng, J. Chang, Y.-W. Tan, J. Li, M. Chen, Y. Sun, F. Li, *Nat. Commun.* **2016**, *7*, 10437; d) C. D. S. Brites, S. Balabhadra, L. D. Carlos, *Adv. Opt. Mater.* **2019**, *7*, 1801239.
- [3] Y. Lu, J. Zhao, R. Zhang, Y. Liu, D. Liu, E. M. Goldys, X. Yang, P. Xi, A. Sunna, J. Lu, Y. Shi, R. C. Leif, Y. Huo, J. Shen, J. A. Piper, J. P. Robinson, D. Jin, *Nat. Photonics* **2014**, *8*, 32.
- [4] a) J. I. Eldridge, T. J. Bencic, D. Zhu, M. D. Cuy, D. E. Wolfe, S. W. Allison, D. L. Beshears, T. P. Jenkins, B. Heeg, R. P. Howard, *NASA Technical Report* **2014**, TM-2014-218418; b) N. Fuhrmann,

- M. Schneider, C. P. Ding, J. Brübach, A. Dreizler, *Meas. Sci. Technol.* **2013**, *24*, 095203; c) S. J. Yi, H. D. Kim, K. C. Kim, *Exp. Therm. Fluid Sci.* **2014**, *59*, 1.
- [5] a) J. F. C. B. Ramalho, S. F. H. Correia, L. Fu, L. L. F. António, C. D. S. Brites, P. S. André, R. A. S. Ferreira, L. D. Carlos, *Adv. Sci.* **2019**, *6*, 1900950; b) J. F. C. B. Ramalho, L. C. F. António, S. F. H. Correia, L. S. Fu, A. S. Pinho, C. D. S. Brites, L. D. Carlos, P. S. André, R. A. S. Ferreira, *Opt. Laser Technol.* **2018**, *101*, 304.
- [6] T. Pan, W. Cao, M. Wang, *Opt. Fiber Technol.* **2018**, *45*, 359.
- [7] a) Q. Mei, H. Jing, Y. Li, W. Yisibashaer, J. Chen, B. Nan Li, Y. Zhang, *Biosens. Bioelectron.* **2016**, *75*, 427; b) A. S. Paterson, B. Raja, V. Mandadi, B. Townsend, M. Lee, A. Buell, B. Vu, J. Brgoch, R. C. Willson, *Lab Chip* **2017**, *17*, 1051; c) H. Kim, Y. Jung, I.-J. Doh, R. A. Lozano-Mahecha, B. Applegate, E. Bae, *Sci. Rep.* **2017**, *7*, 40203; d) A. K. Yetisen, J. L. Martinez-Hurtado, A. Garcia-Melendrez, F. da Cruz Vasconcellos, C. R. Lowe, *Sens. Actuators, B* **2014**, *196*, 156; e) L. Shen, J. A. Hagen, I. Papautsky, *Lab Chip* **2012**, *12*, 4240; f) A. I. Barbosa, P. Gehlot, K. Sidapra, A. D. Edwards, N. M. Reis, *Biosens. Bioelectron.* **2015**, *70*, 5; g) A. Roda, E. Michelini, M. Zangheri, M. Di Fusco, D. Calabria, P. Simoni, *TrAC, Trends Anal. Chem.* **2016**, *79*, 317; h) Q. Wei, R. Nagi, K. Sadeghi, S. Feng, E. Yan, S. J. Ki, R. Caire, D. Tseng, A. Ozcan, *ACS Nano* **2014**, *8*, 1121; i) M. Xiao, Z. Liu, N. Xu, L. Jiang, M. Yang, C. Yi, *ACS Sensors* **2020**, *5*, 870; j) Z. Li, S. Zhang, T. Yu, Z. Dai, Q. Wei, *Anal. Chem.* **2019**, *91*, 10448; k) K. Sun, Y. Yang, H. Zhou, S. Yin, W. Qin, J. Yu, D. T. Chiu, Z. Yuan, X. Zhang, C. Wu, *ACS Nano* **2018**, *12*, 5176; l) N. Cheng, Y. Song, M. M. A. Zeinhom, Y.-C. Chang, L. Sheng, H. Li, D. Du, L. Li, M.-J. Zhu, Y. Luo, W. Xu, Y. Lin, *ACS Appl. Mater. Interfaces* **2017**, *9*, 40671.
- [8] Z. C. Kennedy, D. E. Stephenson, J. F. Christ, T. R. Pope, B. W. Arey, C. A. Barrett, M. G. Warner, *J. Mater. Chem. C* **2017**, *5*, 9570.
- [9] a) Y. Zhou, W. Qin, C. Du, H. Gao, F. Zhu, G. Liang, *Angew. Chem., Int. Ed.* **2019**, *58*, 12102; b) Z. Zhu, *Anal. Chim. Acta* **2019**, *1054*, 122.
- [10] a) L. Li, Y. Zhu, X. Zhou, C. D. S. Brites, D. Ananias, Z. Lin, F. A. A. Paz, J. Rocha, W. Huang, L. D. Carlos, *Adv. Funct. Mater.* **2016**, *26*, 8677; b) J. Rocha, C. D. S. Brites, L. D. Carlos, *Chem. - Eur. J.* **2016**, *22*, 14782; c) G. Bao, K.-L. Wong, D. Jin, P. A. Tanner, *Light: Sci. Appl.* **2018**, *7*, 96; d) Y. Zhang, S. Yuan, G. Day, X. Wang, X. Yang, H.-C. Zhou, *Coord. Chem. Rev.* **2018**, *354*, 28.
- [11] S. Kalytchuk, K. Poláková, Y. Wang, J. P. Froning, K. Cepe, A. L. Rogach, R. Zbořil, *ACS Nano* **2017**, *11*, 1432.
- [12] a) J.-H. Tang, Y. Sun, Z.-L. Gong, Z.-Y. Li, Z. Zhou, H. Wang, X. Li, M. L. Saha, Y.-W. Zhong, P. J. Stang, *J. Am. Chem. Soc.* **2018**, *140*, 7723; b) A. Steinegger, I. Klimant, S. M. Borisov, *Adv. Opt. Mater.* **2017**, *5*, 1700372.
- [13] H. Clevenson, M. E. Trusheim, C. Teale, T. Schröder, D. Braje, D. Englund, *Nat. Phys.* **2015**, *11*, 393.
- [14] M. Sekulić, V. Đorđević, Z. Ristić, M. Medić, M. D. Dramićanin, *Adv. Opt. Mater.* **2018**, *6*, 1800552.
- [15] a) R. V. Alves, K. A. Wickersheim, *Fluoroptical Thermometry: Temperature Sensing Using Optical Fibers*, SPIE, Bellingham, Washington, DC **1984**; b) M. H. Sun, K. A. Wickersheim, J. Kim, *Fiberoptic Temperature Sensors in the Medical Setting*, SPIE, Bellingham, Washington, DC **1989**.
- [16] E. I. Gorokhova, V. A. Demidenko, S. B. Eron'ko, E. A. Oreshchenko, P. A. Rodnyĭ, S. B. Mikhrin, *J. Opt. Technol.* **2010**, *77*, 50.
- [17] J. A. Shepherd, S. M. Gruner, M. W. Tate, M. Tecotzky, *Study of Afterglow in X-Ray Phosphors for Use on Fast-Framing Charge-Coupled Device Detectors*, SPIE, Bellingham, Washington, DC **1997**.
- [18] a) K. Binnemans, *Coord. Chem. Rev.* **2015**, *295*, 1; b) J. Thirumalai, R. Chandramohan, R. Divakar, E. Mohandas, M. Sekar, P. Parameswaran, *Nanotechnology* **2008**, *19*, 395703.
- [19] a) P. F. Smet, J. Botterman, K. Van den Eeckhout, K. Korthout, D. Poelman, *Opt. Mater.* **2014**, *36*, 1913; b) R. Kabe, C. Adachi, *Nature* **2017**, *550*, 384.
- [20] a) H. Mieno, R. Kabe, C. Adachi, *Commun. Chem.* **2018**, *1*, 27; b) W. Zhao, T. S. Cheung, N. Jiang, W. Huang, J. W. Y. Lam, X. Zhang, Z. He, B. Z. Tang, *Nat. Commun.* **2019**, *10*, 1595.
- [21] a) G. R. Peacock, *Temperature Uncertainty of IR Thermal Imager Calibration*, SPIE, Bellingham, Washington, DC **2006**; b) P. R. Muniz, R. d. A. Kalid, S. P. Cani, R. d. S. Magalhães, *Opt. Eng.* **2014**, *53*, 074101.
- [22] A. S. N. Huda, S. Taib, *Appl. Therm. Eng.* **2013**, *61*, 220.
- [23] F. Wang, X. Chen, D. Liu, B. Yang, Y. Dai, *J. Mol. Struct.* **2012**, *1020*, 153.
- [24] J. C. de Mello, H. F. Wittmann, R. H. Friend, *Adv. Mater.* **1997**, *9*, 230.